

Unveiling True Limits of Electrochemical Performance of Organic Cathodes in Multivalent Batteries through Cyclable Symmetric Cells

Olivera Lužanin,^[a, b] Jože Moškon,^{*[a]} Tjaša Pavčnik,^[a, b] Robert Dominko,^[a, b, c] and Jan Bitenc^{*[a, b]}

Multivalent batteries are often hyped as a next-generation high-energy density battery technology, but in reality, both literature reports and practical research are plagued by poor reproducibility of electrochemical results. Within the present work, we take a look at the electrochemical testing of organic cathodes that can be used with a variety of mono- and multivalent cations and propose a cyclable symmetric cell approach, already applied to the field of lithium-ion batteries. By using a model organic system based on poly(anthraquinonyl sulfide) (PAQS) active material, we demonstrate that the symmetric cell approach elegantly removes the limitations of

multivalent metal anodes, and for the first time, reveals the full potential of organic cathodes in multivalent batteries. Furthermore, symmetric cells enable reliable EIS measurements on organic cathodes and open a pathway to optimize electrochemical/transport parameters through the design of next-generation organic cathode materials and advanced electrode design(s). We suggest that the cyclable symmetric cell approach should be generally applicable in multivalent and all other batteries where electrochemical characterization requires the elimination of the counter electrode contribution.

Introduction

High-energy and cost-effective batteries are an essential technology for both electromobility and stationary electrical energy storage applications needed to support the transition from fossil-based energy resources toward renewables. Batteries using multivalent metal anodes meet both requirements while at the same time relying on Earth-abundant elements (Mg, Ca, Al).^[1] However, the practical application of multivalent batteries is severely limited by the performance of multivalent electrolytes and, in particular, by the poor performance of cathode materials. The insertion of multivalent cations is complicated due to the high charge density of multivalent ions, resulting in strong interactions with lattice hosts, slow solid-state diffusion, and a tendency toward conversion reactions

instead of insertion.^[2] As a result, the state-of-the-art cathode for Mg batteries is still a two-decade-old Chevrel phase, Mo_6S_8 , which offers only a low redox potential and a very modest specific capacity.^[3] One way to circumvent the limitations of inorganic hosts is to use organic cathodes with soft and adaptable structures that enable good electrochemical reversibility with various multivalent cations. Although organic cathodes are a good choice for positive electrodes, their performance in combination with multivalent metal anodes is often inferior in terms of capacity utilization and rate capability compared to the monovalent ones (Li, Na, K).^[4,5] To further optimize and develop new organic cathodes that could be paired with multivalent charge carriers in future high-energy density batteries, it is necessary to identify the main culprit for the underwhelming performance of organic cathodes in multivalent batteries. One of the most insightful analytical tools in this task could be electrochemical impedance spectroscopy (EIS), which allows us to monitor electrochemical and transport processes within the battery cell.

The typical electrochemical evaluation of multivalent metal cells is transferred from Li-ion research and performed in two-electrode half-cells, where the multivalent metal anode acts as both reference and counter electrode (RE and CE, respectively) and is present in a large surplus. This approach is sufficient for the majority of alkali metal cells, where metal plating/stripping on the CE occurs with relatively low overpotential. Hence, the electrochemical performance of the cell is indeed limited only by the performance of the cathode material. On the other hand, overpotentials of multivalent metal anodes are much larger, and Mg and Ca metal anodes generally suffer from distinct passivation phenomena, which lead to electrochemical characterization results containing significant contribution of

[a] O. Lužanin, Dr. J. Moškon, T. Pavčnik, Prof. R. Dominko, Dr. J. Bitenc
National Institute of Chemistry
Hajdrihova 19, 1000, Ljubljana, Slovenia
E-mail: joze.moskon@ki.si
jan.bitenc@ki.si

[b] O. Lužanin, T. Pavčnik, Prof. R. Dominko, Dr. J. Bitenc
Faculty of Chemistry and Chemical Technology
University of Ljubljana
Večna pot 113, 1000, Ljubljana, Slovenia

[c] Prof. R. Dominko
Alistore-European Research Institute
CNRS FR 3104, Hub de l'Energie
Rue Baudelocque, 80039, Amiens, France

Supporting information for this article is available on the WWW under <https://doi.org/10.1002/batt.202200437>

An invited contribution to a Special Collection on Organic Batteries

© 2022 The Authors. Batteries & Supercaps published by Wiley-VCH GmbH. This is an open access article under the terms of the Creative Commons Attribution License, which permits use, distribution and reproduction in any medium, provided the original work is properly cited.

the metal anode or even being completely dominated by it. The strong passivation tendency of these types of metal anodes stems from their high reactivity and the insulating nature of the formed surface layers. Furthermore, the presence of even trace amounts of impurities leads to modified and more intense passivation of the metal anode surface.^[6] The presence of a surface passive layer may influence both the redox potential of the multivalent metal anode as well as strongly affect the transport across the anode/electrolyte interface. The latter becomes even more apparent in EIS characterization performed at open circuit conditions, where cell response is more often than not dominated solely by the large magnitude of the passivation resistance of the metal anode and consequently, all the other contributions related to the other electrochemical processes cannot be revealed and studied.

One of the strategies used to remove the effect of CE and ensure reproducible and high-quality electrochemical measurements is the use of a three-electrode setup with a reliable RE. Various cell designs have been proposed for measuring the impedance of 3-electrode Li-ion electrodes.^[7] Nevertheless, there is a generally accepted trade-off that in standard 3-electrode battery cells with RE, the obtained impedance response of the tested electrode is subject to various artifacts.^[8] For example, impedance loops are a clear sign of such distorted spectra due to either geometrical (e.g., different dimensions or mutual misalignment between WE and CE)^[9] or/and electrochemical asymmetry (WE and CE of different nature with different impedance magnitudes or time constants).^[10] However, the issue of finding a suitable and stable RE for multivalent systems is far from trivial and has still not been properly resolved.^[11]

An alternative strategy, which is the focus of this article, is the utilization of a two-electrode symmetric cell approach. More than two decades ago, an approach based on the use of symmetric cells was proposed by Chen et al.^[12,13] to clearly distinguish the contributions of cathode and anode processes to the impedance rise of a full Li-ion cell. With time, symmetric cells have become an invaluable tool in studying low-temperature cell performance,^[14,15] the effects of current collectors,^[16] the dissolution of transition metals,^[17] and in systematic studies of the relationship between the internal resistance and power performance of porous electrodes.^[18–20] Electrode parameters of simple (flat/planar) and porous battery electrodes have recently been studied theoretically and elaborated experimentally using symmetric cells in the framework of various transmission line models (TLMs).^[21–24] In addition, the symmetric cell approach has become an established technique for studying the effects of electrolyte additives and additive combinations.^[25–29] Charge-discharge cycling experiments with symmetric cells are employed to study degradation mechanisms,^[30,31] the effects of electrode calendaring,^[32] as well as the effects of additive on capacity decay.^[33]

Symmetric cell approaches have already been applied to post-Li-ion batteries, for example, in studies of Li–S systems, where they serve as an insightful technique.^[34] Surprisingly, this is not the case for battery systems based on active organic materials. In the present work, we demonstrate that the

practicality of the symmetric cell approach can be elegantly used to study the electrochemical performance and impedance response of organic cathodes in Li-, Mg-, and Ca-battery systems and circumvent the limitations imposed by multivalent metal anodes.

Results and Discussion

Poly(anthraquinonyl sulfide) cathode performance in lithium, magnesium, and calcium

To illustrate the differences in electrochemical performance of the same organic material in different systems, we performed galvanostatic cycling of poly(anthraquinonyl sulfide) (PAQS) electrodes in half-cells versus metal lithium, magnesium, and calcium CEs (Figure 1) at a current rate of C/2. The voltage profile of the first discharge half-cycle differs from subsequent cycles in all cells, which is characteristic of PAQS.^[35,36] PAQS combined with a metal-lithium anode showed excellent capacity retention as well as high Coulombic efficiency (around 99% throughout 100 cycles, Figure S4). At the first discharge, a capacity of 223 mAh g⁻¹ was observed, which corresponds to 92% capacity utilization (theoretical value 225 mAh g⁻¹, for the calculation of PAQS capacity utilization, see discussion in Supporting Information, Figure S5). During the 100 cycles, about 11% of the initial capacity was lost, with an average discharge voltage of about 2.2 V. Cell overpotential of 120 mV remained stable throughout the cycling.

In cells with multivalent metal anodes, significant differences in the performance of the organic cathodes can be observed. Firstly, significantly lower capacity utilization compared to lithium cells is a very notable difference in the electrochemical performance of PAQS versus metallic magnesium and calcium anode. For both cells, only about 50% of the theoretical capacity is (initially) achieved; a performance far inferior to that of the lithium cell. The poor capacity utilization is also accompanied by lower Coulombic efficiency and significantly larger voltage hysteresis (about 780 mV for Mg and 590 mV for Ca, values obtained in the second cycle at C/2) that further increases during the cycling (Figure 1f). PAQS shows poor capacity retention in magnesium, with about 40% of the initial value retained after 100 cycles (Figure S4), accompanied by a larger slope of the voltage curve towards the end of the galvanostatic discharge, which could be possibly related with aggravated ionic transport conditions. Overall, these observations could, hypothetically, be related to the larger overpotential of the Mg metal anode, passivation phenomena at the Mg metal/electrolyte interface, rapid electrolyte decomposition, transport limitations, or degradation of the organic cathode. However, there is no straightforward approach how to differentiate among these contributions and unambiguously assign the dominating phenomena. The half-cell with a calcium metal anode performed even worse. In the case of Ca metal, the reversibility of plating and stripping poses severe limitations to the electrochemical performance of the half-cell.^[4] Only six galvanostatic cycles could be performed

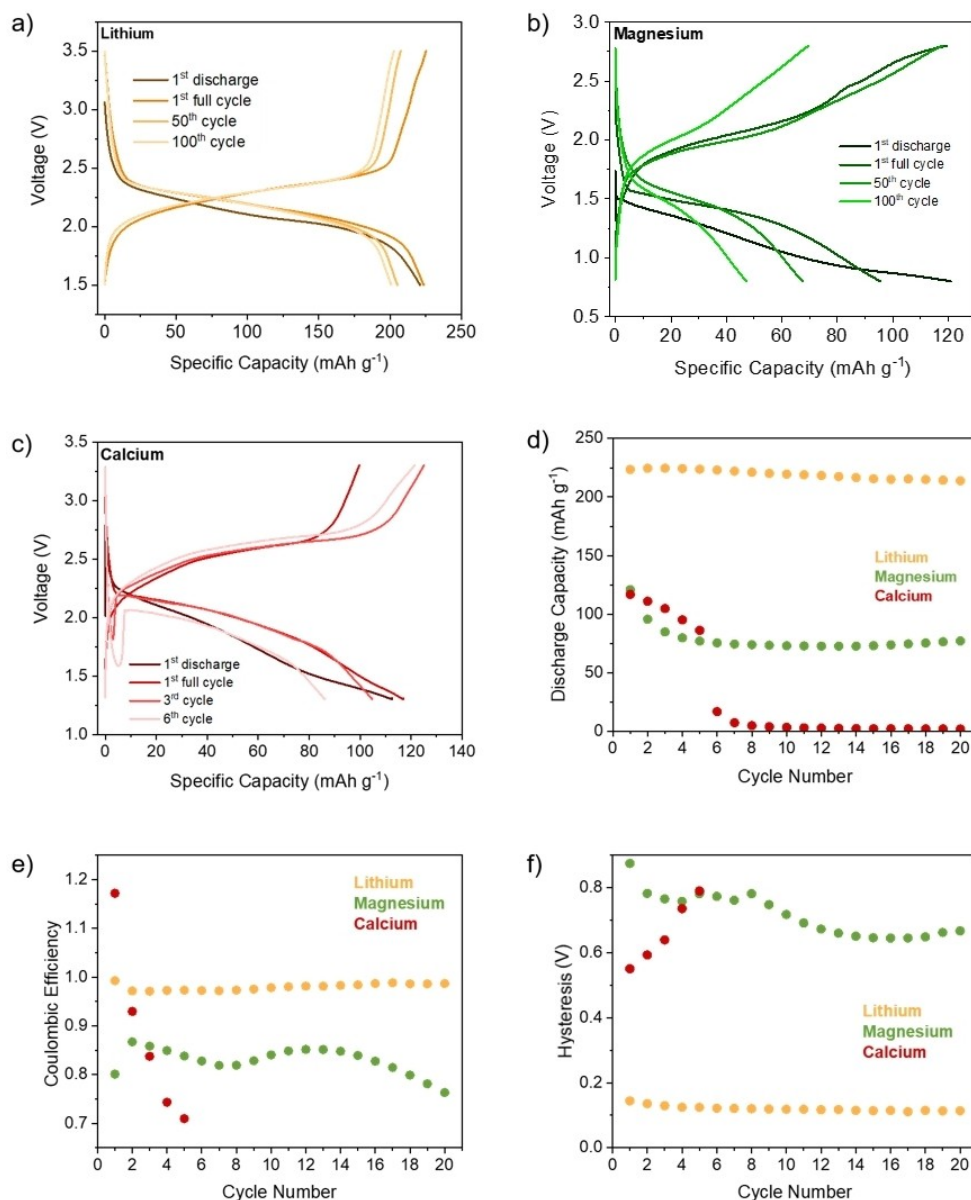


Figure 1. a–c) Measured voltage curves of selected galvanostatic cycles for the PAQS-metal anode cells (metals: Li, Mg, and Ca). Cycling was performed with $C/2$ over 100 cycles. d) Obtained discharge capacities and e) Coulombic efficiencies in the first 20 cycles. f) Corresponding voltage hysteresis for the first 20 cycles (for hysteresis evolution over the 100 cycles, see Figure S6).

before complete cell failure occurred. This phenomenon is associated with the Ca stripping process and can be observed at the beginning of the discharge of the Ca half-cell. During cycling, there is a gradual increase in the overpotential due to the passivation of the Ca metal anode and, finally, the complete failure of the cell.

When EIS is performed on such half-cells, the metal anode response is predominant in the case of cells with Mg and Ca, as evident from spectra of the half-cells with the organic cathode (Figure 2) and spectra of symmetric metal-metal cells (Figure S7). The impedance response of the multivalent metal anode completely conceals the response of the organic cathode, and discrimination between the response of the WE and the CE is impossible in most cases. Moreover, both the

half-cells (Figure 2) as well as the symmetric cells (Figure S7) that include Mg and Ca metal exhibit instabilities (scattered data and drift) in the low-frequency part of the spectra. It has been suggested that, for impedance measurements, Ca and Mg metal electrodes should not be used as CE or RE in both two- and three-electrode configurations because their generally high impedance could lead to significant errors or artifact loops.^[11] Therefore, it is obvious that a different type of reliable electrochemical setup must be devised to obtain meaningful responses for the EIS measurement of organic cathodes in multivalent batteries.

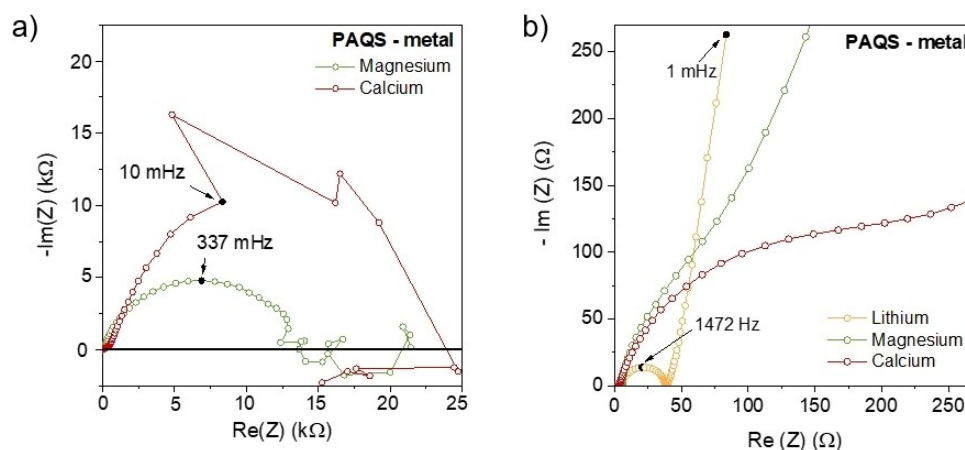


Figure 2. a) Nyquist plots of measured PEIS responses of PAQS-metal cells at SoC=0.5 (metal anode = Li, Mg, Ca) with the full frequency span shown (1 MHz–1 mHz). Note that Li-PAQS PEIS response is not visible because of the large resistance of multivalent metals. b) Inset showing the part of the spectra where PEIS response of Li-PAQS cell is visible.

Overcoming the issues of unstable CEs

Several methods have been developed to avoid the problems associated with using Mg and Ca as CEs. For example, instead of a metal electrode activated carbon (AC) can be used as a CE.^[37,38] The main principle of operation of a cell with AC as CE (in the case of our quinone-type compounds and n-type cathode compounds in general) is that during the discharge of cathode materials, when cations are stored inside the cathode, simultaneously, there is an accumulation of positive charge on the surface of carbon and storage of salt anions in the double layer of CE. The open circuit voltage of activated carbon electrodes is relatively high, about 3 V vs. Li/Li⁺. Consequently, when this type of electrode is paired with an organic electrode, and the organic electrode is discharged, the AC can quickly exceed the stability window of the electrolyte. This is particularly problematic for glyme-based electrolytes with limited oxidative stability. In addition, this type of capacitive CE has a low specific capacity, and accordingly, due to the purely capacitive nature of the charge storage, its potential can vary significantly during electrochemical cycling. Therefore, the introduction of CE based on AC might bring in the electrochemical characterization some serious limitations by itself and cannot provide a defined and stable reference potential.

An alternative approach for removing the limitations of CE and a proven method for obtaining accurate impedance measurements is the implementation of a symmetric cell approach. In this setup, two nominally identical electrodes are concomitantly subjected to impedance perturbation and the series addition of the impedance of the single electrode is effectively measured. If there is a very large deviation between the electrodes, errors are introduced for single electrode parameter values with simple “averaging” of the cell response. In practice, it is easy to prepare electrodes with a mass deviation of less than 5% thus the accuracy of the obtained parameter values is reasonably high. But most importantly, no matter how large the (mass/parameter) deviation between the

electrodes is, the measured response of the cell does not include artifacts.

In this work, we refer to symmetric cells consisting of two electrodes with the same composition and state of charge as *conventional* symmetric cells and cells consisting of two electrodes of the same composition and different state of charge, one of which was previously discharged and the other in the pristine (or charged) state as *cyclable* symmetric cells.

Cyclable symmetric cells with organic electrodes

Although it functions in principle, the standard approach of conventional symmetric cell preparation has some shortcomings. Namely, it is time-consuming to assemble three starting half-cells (one serves as a backup cell) and afterward the corresponding symmetric cell. Furthermore, the conventional symmetric cell approach becomes more problematic when multivalent metals are used. The performance of the cells with multivalent metals is more susceptible to the pretreatment of magnesium and calcium metal anodes and the quality of electrolyte, resulting in worse reproducibility of the galvanostatic performance of the half-cells. From the point of view of gaining a deeper understanding of the operation of organic cathodes in studied (Li, Mg, Ca) electrolytes, it is of major importance to perform cycling and EIS measurements on the same cell.

For this reason, we are using cyclable symmetric cells which are a special case of symmetric cells. The type of symmetric cells used in the present study enables full-capacity cycling testing. Instead of preparing two nominally identical initial cathode-anode half-cells at the selected SoC, we had, in the first step, prepared only one starting half-cell that was discharged (for the details, see the Experimental). In the following step, the initially discharged electrode (for example electrode A) was paired with the second – but in this case pristine – electrode (for example electrode B), as schematically shown in Figures 3a and S8. The polarity of the electrodes in the

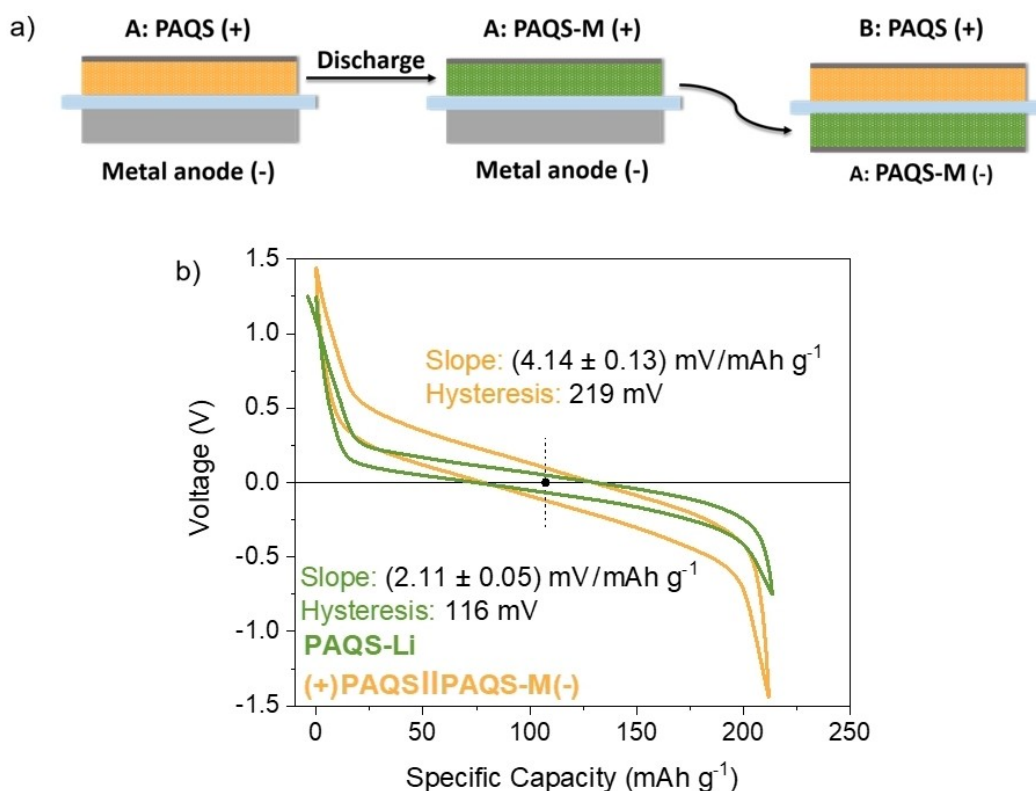


Figure 3. a) Scheme showing the preparation of a cyclable PAQS symmetric battery cell. b) Proof of concept showing measured (galvanostatic) voltage hysteresis of PAQS–Li and (+)PAQS || PAQS–M(–) cell in 1 M LiTFSI in DOL/DME obtained at C/5. The magnitude of voltage hysteresis and the slope of the voltage curve correspond to SoC = 0.5 (2.22 V vs. Li and 0 V for cyclable symmetric cell).

obtained symmetric cell B(+)|A(–) is the following: the discharged electrode A has a lower potential (–) compared to the pristine electrode B (+). This type of symmetric cell enables the performance of galvanostatic (or any other type of) electrochemical characterization since the coordinated cation (initially stored) within electrode A can be reversibly moved to electrode B and vice versa. This cyclable symmetric cell setup should be distinguished from symmetric all organic battery, as PAQS contains only one type of active center.^[39]

To prove that the cyclable symmetric organic cells are a viable electrochemical setup, we compared the voltage hysteresis of a PAQS–Li half-cell with the voltage hysteresis of a cyclable symmetric (+)PAQS || PAQS–M(–) cell. Voltage hysteresis and slope of the voltage curve should be doubled compared to the values obtained in a half-cell. This is a prerequisite for the verification of the underlying principle: in the symmetric cell we are driving reaction and transport processes in the two electrodes simultaneously (mirrored symmetrically) in both directions during each half-cycle (see Figure S9). Accordingly, the insights obtained in the impedance can be directly related to the galvanostatic performance. Figure 3(b) shows the comparison of a typical (galvanostatic) voltage hysteresis of PAQS–Li cell (green) and symmetric (+)PAQS || PAQS–M(–) cell (orange) obtained in 1 M LiTFSI in DOL/DME at C/5 rate. Note that, for the purpose of direct optical analysis of the data, the voltage curves of the PAQS–Li cell were shifted down by the voltage axis for a value of 2.22 V

for the central point of the hysteresis to be aligned with the hysteresis of the symmetric cell. (For unshifted voltage curve comparison, see Figure S9). The magnitude of the shift (2.22 V) represents the equilibrium voltage of PAQS in the lithium cell at the central point (SoC = 0.5). At the selected central point of the hysteresis of the PAQS–Li and the symmetric cell, one obtains the following values of hysteresis and slope: 116 mV vs. 219 mV and $(2.11 \pm 0.05) \text{ mV}/(\text{mAh g}^{-1})$ vs. $(4.14 \pm 0.13) \text{ mV}/(\text{mAh g}^{-1})$. The analysis was performed by doing linear regression in the central part of the centered voltage curves ($95\text{--}120 \text{ mAh g}^{-1}$) and the reported values for the slopes are the average of the charge and discharge (positive/negative current) values (Figures S13–S15). Both the hysteresis and the slope values of the symmetric cell are very close to double the values corresponding to the PAQS–Li cell. In fact, one-quarter of the hysteresis of the symmetric cell ($0.25 \times 219 \text{ mV} = 55 \text{ mV}$) is the more exact value of PAQS electrode overpotential than the one obtained in the PAQS–Li cell ($0.5 \times 116 \text{ mV} = 58 \text{ mV}$) since it does not include the overpotential of Li metal CE. The latter seems to have a small (few mV) yet measurable contribution (for more discussion see Supporting Information). As shown in the continuation, the contribution of Mg and Ca metal CE to the measured hysteresis of the corresponding half-cells is much larger and thus gives seriously overestimated values of the cathode overpotential if CE is not properly considered.

Figure 4 shows the comparison of the galvanostatic performance of cyclable symmetric organic ((+)PAQS || PAQS-M(-)) cells in lithium, magnesium, and calcium electrolytes (for direct comparison of symmetric cell voltage hysteresis at C/2 in three electrolytes, see Figure S10). Starting with the PAQS electrodes in lithium electrolyte (Figure 4a and d), excellent rate performance is observed with 147 mAh g^{-1} obtained at 50 C. For comparison, the capacity values obtained at the same current rate in a PAQS-Li half-cell (Figure S11) are about 63 mAh g^{-1} . This excellent rate capability shows that, although lithium half-cells are the least problematic in terms of CE passivation and electrolyte stability, symmetric cells can still reveal important insights and thus can be considered a helpful tool for studying organic cathodes in lithium electrolytes. At

high rates, the formation of dendrites and (partially passivated) high surface-area porous lithium layer can limit the electrochemical performance of lithium metal. As demonstrated, by eliminating the metal anode, more direct insight can be gained into the performance of organic cathodes at high rates. PAQS exhibits similar behavior in symmetric cells with multivalent electrolytes, with overall poorer rate performance than in lithium electrolyte (Figure 4a–d). Interestingly, the magnitude of voltage hysteresis of PAQS in the calcium electrolyte (417 mV at C/5) is smaller compared to the magnesium electrolyte (590 mV at C/5) at all rates (Figures S10 and S12, and Table S1), which is an observation that is inaccessible in a cathode-metal anode setup. Moreover, as it can be deduced from Figures 1(f) and S12, the overpotential of PAQS electrodes

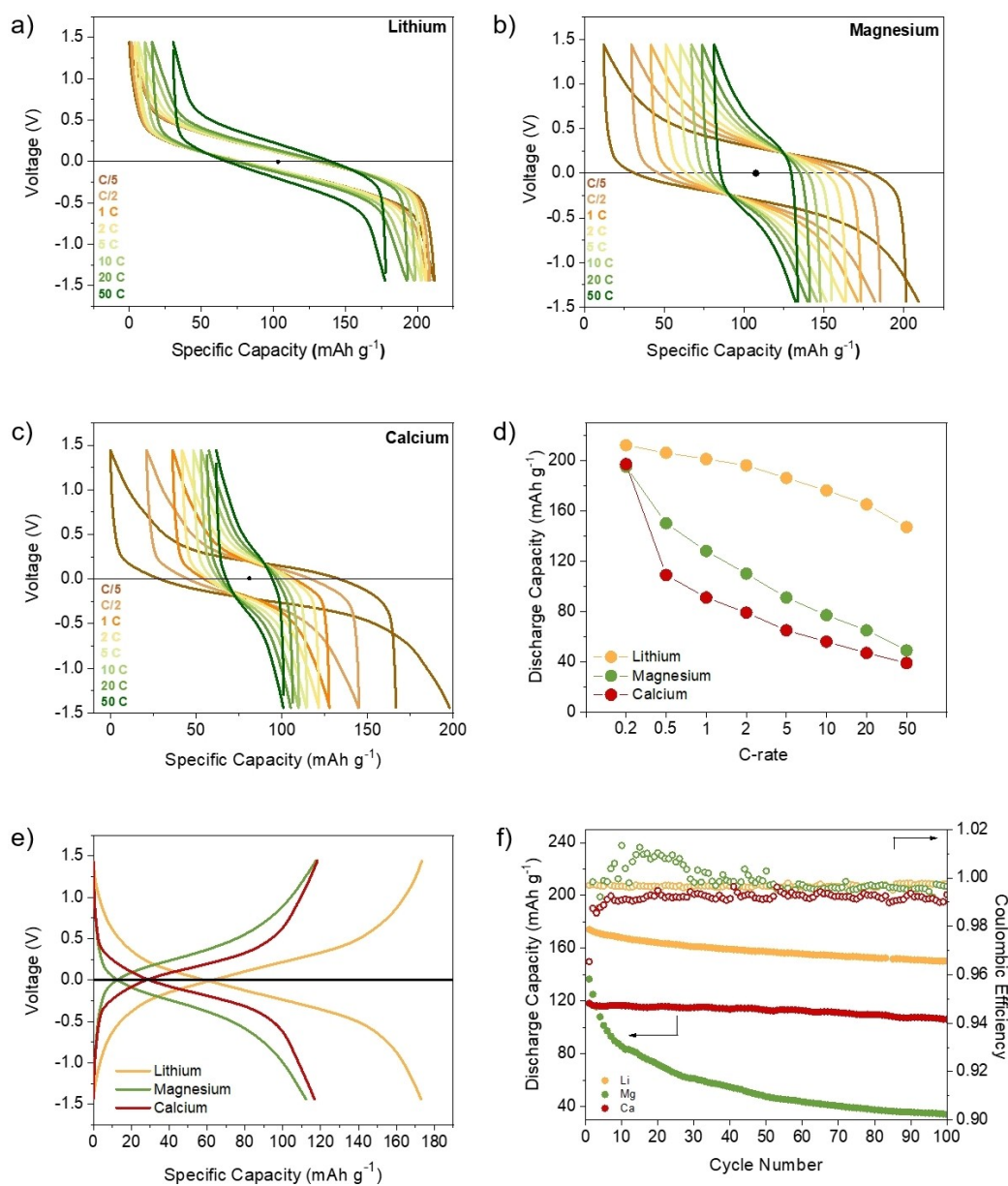


Figure 4. a) Cyclable (+)PAQS || PAQS-M(-) cells—voltage hysteresis at different C-rates in lithium, b) magnesium, and c) calcium electrolyte. d) Discharge capacity at different C-rates. e) Selected galvanostatic cycles of the organic (+)PAQS || PAQS-M(-) cells measured at C/2. f) Cycling stability (full circles) and Coulombic efficiency (hollow circles) of symmetric cells during 100 cycles at C/2.

in symmetric cells is much smaller compared to the overpotential observed in the corresponding Mg and Ca half-cells (Table S1). For example, for the case of C/2 rate, the obtained overpotentials of the PAQS electrodes in the symmetric cells were: $0.25 \times 214 \text{ mV} = 54 \text{ mV}$ (Li), $0.25 \times 389 \text{ mV} = 97 \text{ mV}$ (Ca), and $0.25 \times 627 \text{ mV} = 157 \text{ mV}$ (Mg), respectively. The overpotentials of the PAQS electrodes in the corresponding half-cells cells were: 56 mV (Li), 295 mV (Ca), and 389 mV (Mg). The latter observation is an additional confirmation that strong passivation phenomena and related instability issues of multivalent metal anodes in Mg and Ca battery systems prevent access to the actual electrochemical response and performance of studied cathodes. As for the performance at different C-rates, symmetric cells in the Mg and Ca electrolytes show a similar trend whereby the cell in the Mg electrolyte slightly outperformed the one in Ca (Figure 4d), with both cells reaching about 90% of the theoretical value at 0.5 C and about 20% of the theoretical value at 50 C. When we compare the cycling stability of the symmetric (+)PAQS || PAQS-M(-) cells in calcium and magnesium electrolytes at C/2 over 100 cycles (Figure 4f), capacity retention is significantly better in calcium electrolyte, where around 90% of the initial capacity is retained compared to just 25% for the magnesium cell. There could be several different origins for the observed difference in the evolution of the cycling stability – for example, the effect of Mg complexation species leading to decreased stability of Mg electrolyte, increased solubility in Mg electrolyte, or some other effect. The better stability of the symmetric cell cycling in calcium electrolyte is also reflected in more stable Coulombic efficiency. Note that the voltage window chosen for cyclable symmetric cells was derived from the performance of the lithium half-cell. As this study serves merely as a proof of concept, further optimization of the voltage window is required for multivalent cells to achieve optimization of their electrochemical performance. Whatever the detailed mechanism behind the evidently different cycling stability of PAQS-based electrodes in Mg and Ca electrolytes, this kind of information is new and could not be obtained from the cycling performance

of the corresponding PAQS-metal anode half-cells (see Figure 1).

Impedance responses of cyclable (+)PAQS || PAQS-M(-) symmetric cells were measured at SoC=0.5 in a frequency span from 1 MHz to 1 mHz (identical measurement conditions as used for the corresponding half-cells, Figure 2). Obtained Nyquist plots of the measured PEIS in Li, Mg, and Ca electrolytes are shown comparatively in Figure 5. When comparing EIS spectra obtained in a symmetric configuration with the ones obtained in cells with the metal anode it can clearly be seen that in the case of Mg and Ca, the impedance magnitudes of the symmetric cells are much smaller compared to the large impedance (resistance) contribution of passive layers of the corresponding (Mg, Ca) metal anodes. It has to be noted that for a fair comparison of the impedance magnitudes, the EIS spectra of the symmetric cells should be halved – to obtain the impedance response of a single electrode. Accordingly, the largest impedance magnitude, $|Z|$, for the (single) electrode in the Mg symmetric cell (Figure 5) at 1 mHz is about 1 k Ω . In the corresponding PAQS-Mg metal cell the obtained impedance magnitude approaching 1 mHz showed scattered values and reached about 20 k Ω . Similar observations can be found for the symmetric and PAQS-Ca metal cell in the Ca electrolyte. Secondly, the obtained EIS data of the multivalent (+)PAQS || PAQS-M(-) symmetric cells exhibit spectra with “smooth” frequency dependence and low noise level, indicating good quality and stable impedance response of the symmetric cells.

The EIS spectra of the PAQS electrodes in the three studied electrolytes (Figure 5) share some common traits. Firstly, a small or even no visible arc at high frequencies (in the range of about 100–10 kHz) indicates good electronic contact between the current collector (carbon-coated aluminum foil) and the electrode composite, obtained by the electrode pressing step (see Experimental), which is in agreement with the observations found for Li-ion battery cathodes.^[40,41] The typical close-to 45° inclined-line feature in the frequency ranges from about a few kHz down to about 30 Hz (the knee-like transition) visible in all the spectra (Figure 5b) reveals that the ionic resistance of the electrolyte phase in the voids and pores of the porous

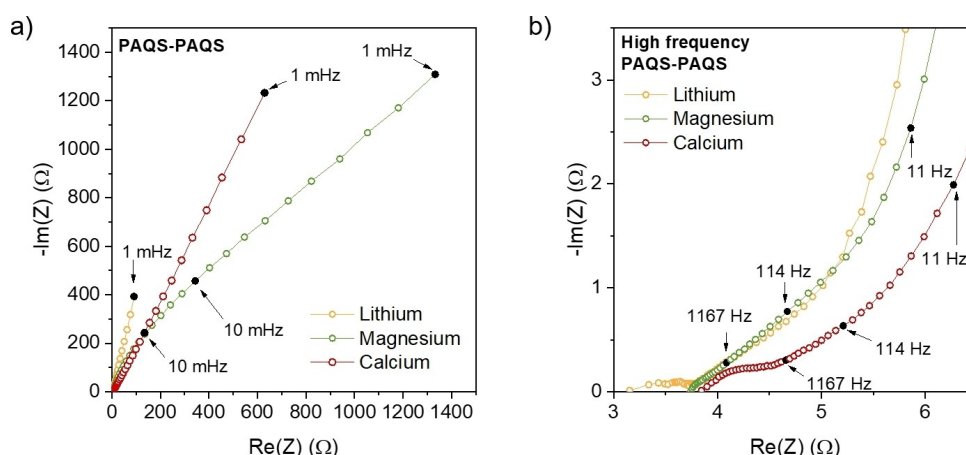


Figure 5. Typical Nyquist plots of measured PEIS responses of (+)PAQS || PAQS-M(-) cyclable symmetric cells obtained at SoC = 0.5.

electrodes is reasonably low, with the typical values of about 1.5–2 Ω (for the two electrodes in series). Somewhat surprisingly, both 0.2 M Mg[B(hfip)₄]₂ and Ca[B(hfip)₄]₂ in DME exhibit comparable ionic resistances in the electrode pores, as does 1 M LiTFSI DOL:DME (1:1, v:v), indicating excellent ionic conductivity of these multivalent electrolytes at relatively low concentrations. This is in agreement with the reported data for bulk electrolyte conductivity.^[42] Finally, the general response in medium- and low-frequency regions exhibits distribution behavior that somewhat roughly resembles the (hypothetical) Constant-Phase-Element (CPE) response. Notably, the associated (distributed) resistive contribution grows in the order: Li < Ca < Mg; with total values of about 95, 630, and 1330 Ω at 1 mHz, respectively. In general, this trend suggests that a possible diffusion-type charge storage mechanism within PAQS particles presents large associated resistance for the Mg species and about half smaller for the Ca species, while for the Li species (presumably Li⁺ ions) it presents at least an order of magnitude smaller obstacle. The data presented here are insufficient to reveal more about the nature of the transport and probably coupled synchronous redox switching of the carbonyl centers. Interestingly, and quite surprisingly, none of the spectra in Figure 5 show a distinctive impedance arc that could be associated with the desolvation and charge incorporation process at the interface between the active organic material and the electrolyte.

The comparison of the EIS data for the symmetric cells (Figure 5) and the corresponding half-cells (Figure 2) clearly demonstrates that the multivalent half-cell data cannot be used for determining the impedance properties of the cathodes – but fortunately, the symmetric cell approach enables us to circumvent this issue. Further work is ongoing to explore the full power of the symmetric cell approach, where the galvanostatic performance of organic cathodes will be directly related to the corresponding impedance parameters that will be explored with the help of novel transmission-line models and finally explained on a physical basis.

Conclusion

Organic electrode materials are being intensively investigated as cathodes in multivalent metal anode batteries for future high-energy-density applications. However, their electrochemical characterization in multivalent systems is most often performed in two-electrode metal anode half-cells which, due to the limitations of multivalent metal anodes, does not reveal their full electrochemical performance. In this work, we show that metal anode limitations can be successfully avoided by the preparation and electrochemical characterization of cyclable symmetric cells. This relatively simple type of cell allows us to map the previously inaccessible electrochemical activity of organic electrodes in Ca electrolyte, and organic electrodes in both Ca and Mg electrolyte sat at exceptionally high rates up to 50 C. Cycling at high rates shows that organic electrodes can act as high-power cathodes in a multivalent electrolyte system. Moreover, we observed that Li metal anode CE can have a

dominant contribution in the metal-organic cells at such high current densities. Besides enabling reliable galvanostatic characterization – by accessing the intrinsic performance of organic cathodes – cyclable symmetric setups open up the opportunity for advanced EIS characterization. Most notably, the EIS of organic electrodes reveals various contributions belonging to ionic resistance in electrodes and reveals a diffusion-type charge storage mechanism within the active particles. Organic cathodes exhibit specific differences in the shape and magnitude of impedance response when interacting with Li, Mg, and Ca species. The magnitude of the low-frequency contributions is in direct correlation with the magnitude of the corresponding voltage hysteresis (cathode overpotential). These properties could not be measured in a conventional half-cell setup and will enable future detailed studies of the electrochemical mechanism of organic electrodes in various electrolytes. We believe that the developed methodology should find broad applicability in the multivalent battery field and all other battery applications, where dominant overpotentials of CE electrodes are limiting the performance of the tested cell and thus preventing accessing the true performance of studied WE. Lastly, we believe that the use of the symmetric cell approach will improve the comparability of the obtained results within the field by eliminating the role of the (metal) anode/electrolyte interface in the electrochemical testing of electrode materials.

Experimental

Materials

1,5-dichloroanthraquinone (Alfa Aesar, 96%), N-methyl-2-pyrrolidone (NMP) (Merck, reagent grade, 99%), multi-walled carbon nanotubes (MWCNTs) (NanoTechLabs, C-grade), polytetrafluoroethylene (PTFE, Sigma-Aldrich, 60% water dispersion), NaBH₄ (Sigma-Aldrich, $\geq 98.0\%$), and Ca(BH₄)₂·THF (Sigma-Aldrich), were used as received. Na₂S·xH₂O (Sigma-Aldrich, min. 60% water content) was first subjected to azeotropic distillation in toluene (water content 40%) and then dried under vacuum for 24 h (150 °C). 1,1,1,3,3,3-hexafluoro-2-propanol (H-hfip) (Apollo Scientific, 99.9%) and hexane (Carlo Erba) were both dried with 4 Å molecular sieves for 7 days prior to use. 1,2-dimethoxyethane (DME) (Sigma-Aldrich, HPLC grade, 99.9%) and 1,3-dioxolane (DOL) (Acros, 99.8%) were dried with 4 Å molecular sieves for several days, refluxed with Na/K alloy (ca. 1 ml l⁻¹) overnight, and then fractionally distilled. The final water content in distilled solvents was below 1 ppm as determined by Karl-Fischer titration. LiTFSI salt (TFSI-bis(trifluoromethanesulfonyl)imide, Sigma-Aldrich, 99.95%) was dried at 180 °C under a vacuum overnight.

Polymer and salt synthesis and characterization

Mg[B(hfip)₄]₂ and Ca[B(hfip)₄]₂ salts were synthesized through the previously published procedures,^[4,43] with the addition of salt precipitation in the isolation step. Details are provided in Supporting Information. Prepared salts were characterized by IR and NMR spectroscopy. IR characterization was performed under an inert atmosphere using an ATR-IR Alpha II (Bruker) equipped with a Ge crystal. Measurements were collected and averaged over 48 scans in the range between 2000 and 600 cm⁻¹. Spectra are

provided in Supporting Information (Figures S1 and S2). ^1H and ^{19}F NMR spectra were measured on a Bruker AVANCE NEO 600 MHz NMR spectrometer using DMSO- d_6 solvent.

Electrolytes were prepared by weighing the appropriate amount of salts into volumetric flasks and diluting them up to the mark, obtaining 0.2 M $\text{Mg}[\text{B}(\text{hfp})_4]_2$, 0.2 M $\text{Ca}[\text{B}(\text{hfp})_4]_2$ in DME, and 1 M LiTFSI in a mixture of DOL and DME (1:1, v/v).

All synthesis procedures and electrolyte preparation were carried out in an Ar-filled glovebox, with water and oxygen levels below 0.1 ppm.

PAQS composite was synthesized according to the previously reported polycondensation reaction with the addition of MWCNTs in situ.^[35] Obtained polymer composite was characterized by IR spectroscopy (Figure S3).

Electrode fabrication and cell assembly

PAQS/CNT powder was mixed with Printex XE2 and PTFE in a weight ratio of 6:3:1 in a dispersion of isopropanol. The mixture was then subjected to planetary ball milling for 30 minutes on Retsch PM100 at 300 rpm. Obtained soft plastic composite was rolled between the glass plate and parchment paper, and 12 mm self-standing electrodes were cut (1.13 cm^2). Electrodes were then pressed on carbon-coated aluminum foil (0.9 t per 1 cm^2 , 30 s), dried under vacuum at 50°C , and transferred inside an Ar-filled glovebox. Mass loading of the active material ranged between $1.5\text{--}2.0\text{ mg cm}^{-2}$.

All of the electrochemical experiments were performed in Swagelok-type cells. In lithium cells, one glassy fiber GF/A (Whatman, 260 μm , 13 mm) and one Celgard 2320 (13 mm) were used as separators and soaked with 65 μL of electrolyte. Lithium foil (110 μm , FMC) was rolled until achieving fine shine, cut into 12 mm discs and used as the anode. In magnesium and calcium cells two GF/A glassy fiber separators were used per cell and soaked with 130 μL of magnesium or calcium-based electrolyte. Mg foil (Changsha Rich Nonferrous metals, 99.95%, 0.1 mm) was brushed with P1200 sandpaper and cut into a 12 mm disc cell before cell assembly. Calcium shots (Alfa Aesar, 1 cm and down, 99%) were punched into 12 mm discs and scratched with a spatula until a shiny surface was revealed and used as metal anodes.

Electrochemical measurements

All the galvanostatic and electrochemical impedance experiments were performed using a VMP3 Bio-Logic potentiostat/galvanostat controlled by EC-Lab[®] software. All of the cells were assembled inside an Ar-filled glovebox. Galvanostatic cycling on full cells was done in potential windows 1.5–3.5 V, 1.3–3.3 V, and 0.8–2.8 V for lithium, calcium, and magnesium, respectively. For symmetric cells, cycling was done in the potential window from -1.44 to 1.44 V . Applied currents for rate capability testing were C/5, C/2, 1 C, 2 C, 5 C, 10 C, 20 C, and 50 C.

Pre-cycling of PAQS cathodes was done versus metal lithium, magnesium, and calcium, by discharging the cells down to 1.5-, 0.8, and 1.3 V, respectively, with C/10. Voltage was then held for 12 h (current drops to the value lower than the one corresponding to C/100). Cells were then transferred inside an Ar-filled glovebox, and paired with fresh PAQS electrode. One fresh GF/A glassy fiber separator was used, with the addition of 80 μL of fresh electrolyte. Electrode masses of precycled and fresh PAQS electrodes did not differ by more than 5%.

In potentiostatic impedance measurements (PEIS), sinusoidal perturbation with an amplitude of 5 mV (peak value) was applied in a frequency span from 1 MHz down to 1 mHz, with 10 points per decade of the frequency sweep. All of the measurements were performed at room temperature.

Acknowledgements

The authors would like to acknowledge the financial support from the European Union's Horizon 2020 innovative training program under Marie Skłodowska Curie actions Grant agreement No. 860403 and Slovenian Research Agency through research programme P2-0423 and project J2-4462.

Conflict of Interest

The authors declare no conflict of interest.

Data Availability Statement

The data that support the findings of this study are available from the corresponding author upon reasonable request.

Keywords: electrochemical impedance spectroscopy · metal anodes · multivalent batteries · organic cathode · symmetric cells

- [1] A. Ponrouch, J. Bitenc, R. Dominko, N. Lindahl, P. Johansson, M. R. Palacin, *Energy Storage Mater.* **2019**, *20*, 253–262.
- [2] P. Canepa, G. Sai Gautam, D. C. Hannah, R. Malik, M. Liu, K. G. Gallagher, K. A. Persson, G. Ceder, *Chem. Rev.* **2017**, *117*, 4287–4341.
- [3] D. Aurbach, Z. Lu, A. Schechter, Y. Gofer, H. Gizbar, R. Turgeman, Y. Cohen, M. Moshkovich, E. Levi, *Nature* **2000**, *407*, 724–727.
- [4] J. Bitenc, A. Scafuri, K. Pirnat, M. Lozinšek, I. Jerman, J. Grdadolnik, B. Fraisse, R. Berthelot, L. Stievano, R. Dominko, *Batteries & Supercaps* **2021**, *4*, 214–220.
- [5] H. Wang, M. Mao, C. Wang, *Macromol. Rapid Commun.* **2022**, 2200198.
- [6] J. G. Connell, B. Genorio, P. P. Lopes, D. Strmcnik, V. R. Stamenkovic, N. M. Markovic, *Chem. Mater.* **2016**, *28*, 8268–8277.
- [7] J. Y. Song, H. H. Lee, Y. Y. Wang, C. C. Wan, *J. Power Sources* **2002**, *111*, 255–267.
- [8] M. D. Levi, V. Dargel, Y. Shilina, D. Aurbach, I. C. Halalay, *Electrochim. Acta* **2014**, *149*, 126–135.
- [9] M. Ender, A. Weber, I.-T. Ellen, *J. Electrochem. Soc.* **2011**, *159*, A128–A136.
- [10] S. Klink, E. Madej, E. Ventosa, A. Lindner, W. Schuhmann, F. La Mantia, *Electrochem. Commun.* **2012**, *22*, 120–123.
- [11] R. Dugas, J. D. Forero-Saboya, A. Ponrouch, *Chem. Mater.* **2019**, *31*, 8613–8628.
- [12] M. Adamič, S. D. Talian, A. R. Sinigoj, I. Humar, J. Moškon, M. Gaberšček, *J. Electrochem. Soc.* **2019**, *166*, A5045–A5053.
- [13] C. H. Chen, J. Liu, K. Amine, *J. Power Sources* **2001**, *96*, 321–328.
- [14] S. S. Zhang, K. Xu, T. R. Jow, *J. Power Sources* **2003**, *115*, 137–140.
- [15] N. Ogihara, Y. Itou, S. Kawauchi, *J. Phys. Chem. Lett.* **2019**, *10*, 5013–5018.
- [16] N. Schweikert, H. Hahn, S. Indris, *Phys. Chem. Chem. Phys.* **2011**, *13*, 6234.
- [17] H. Nara, K. Morita, T. Yokoshima, D. Mukoyama, T. Momma, T. Osaka, *AIMS Mater. Sci.* **2016**, *3*, 448–459.
- [18] N. Ogihara, S. Kawauchi, C. Okuda, Y. Itou, Y. Takeuchi, Y. Ukyo, *J. Electrochem. Soc.* **2012**, *159*, A1034–A1039.

- [19] N. Ogihara, Y. Itou, T. Sasaki, Y. Takeuchi, *J. Phys. Chem. C* **2015**, *119*, 4612–4619.
- [20] Y. Itou, N. Ogihara, S. Kawauchi, *J. Phys. Chem. C* **2020**, *124*, 5559–5564.
- [21] M. Adamič, S. D. Talian, A. R. Sinigoj, I. Humar, J. Moškon, M. Gaberšček, *J. Electrochem. Soc.* **2019**, *166*, A5045–A5053.
- [22] S. Drvarič Talian, J. Moškon, R. Dominko, M. Gaberšček, *Electrochim. Acta* **2019**, *302*, 169–179.
- [23] J. Moškon, J. Žuntar, S. Drvarič Talian, R. Dominko, M. Gaberšček, *J. Electrochem. Soc.* **2020**, *167*, 140539.
- [24] J. Moškon, M. Gaberšček, *J. Power Sources Adv.* **2021**, *7*, 100047.
- [25] D. Applestone, A. Manthiram, *J. Power Sources* **2012**, *217*, 1–5.
- [26] P. Ping, Q. S. Wang, J. H. Sun, X. Xia, J. R. Dahn, *J. Electrochem. Soc.* **2012**, *159*, A1467–A1473.
- [27] R. Petibon, C. P. Aiken, N. N. Sinha, J. C. Burns, H. Ye, C. M. VanElzen, G. Jain, S. Trussler, J. R. Dahn, *J. Electrochem. Soc.* **2013**, *160*, A117–A124.
- [28] R. Petibon, N. N. Sinha, J. C. Burns, C. P. Aiken, H. Ye, C. M. VanElzen, G. Jain, S. Trussler, J. R. Dahn, *J. Power Sources* **2014**, *251*, 187–194.
- [29] Y. Liu, I. Hamam, J. R. Dahn, *J. Electrochem. Soc.* **2020**, *167*, 110527.
- [30] J. C. Burns, L. J. Krause, D.-B. Le, L. D. Jensen, A. J. Smith, D. Xiong, J. R. Dahn, *J. Electrochem. Soc.* **2011**, *158*, A1417–A1422.
- [31] L. J. Krause, L. D. Jensen, J. R. Dahn, *J. Electrochem. Soc.* **2012**, *159*, A937–A943.
- [32] A. van Bommel, R. Divigalpitiya, *J. Electrochem. Soc.* **2012**, *159*, A1791–A1795.
- [33] C. Shen, D. Xiong, L. D. Ellis, K. L. Gering, L. Huang, J. R. Dahn, *J. Electrochem. Soc.* **2017**, *164*, A3349–A3356.
- [34] S. Drvarič Talian, J. Moskon, R. Dominko, M. Gaberšček, *ACS Appl. Mater. Interfaces* **2017**, *9*, 29760–29770.
- [35] Z. Song, H. Zhan, Y. Zhou, *Chem. Commun.* **2009**, 448–450.
- [36] J. Bitenc, K. Pirnat, T. Bančič, M. Gaberšček, B. Genorio, A. Randon-Vitanova, R. Dominko, *ChemSusChem* **2015**, *8*, 4128–4132.
- [37] M. Cabello, F. Nacimiento, R. Alcántara, P. Lavela, C. Pérez Vicente, J. L. Tirado, *Chem. Mater.* **2018**, *30*, 5853–5861.
- [38] X. Sun, V. Duffort, B. L. Mehdi, N. D. Browning, L. F. Nazar, *Chem. Mater.* **2016**, *28*, 534–542.
- [39] Z. Li, Q. Jia, Y. Chen, K. Fan, C. Zhang, G. Zhang, M. Xu, M. Mao, J. Ma, W. Hu, C. Wang, *Angew. Chem. Int. Ed.* **2022**, *33*, e202207221.
- [40] J.-M. Atebamba, J. Moskon, S. Pejovnik, M. Gaberscek, *J. Electrochem. Soc.* **2010**, *157*, A1218–A1228.
- [41] M. Gaberscek, J. Moskon, B. Erjavec, R. Dominko, J. Jamnik, *Electrochem. Solid-State Lett.* **2008**, *11*, A170–A174.
- [42] T. Mandai, Y. Youn, Y. Tateyama, *Mater Adv* **2021**, *2*, 6283–6296.
- [43] Z. Zhao-Karger, M. E. Gil Bardaji, O. Fuhr, M. Fichtner, *J. Mater. Chem. A* **2017**, *5*, 10815–10820.

Manuscript received: September 30, 2022
Revised manuscript received: November 15, 2022
Version of record online: December 5, 2022